J. Fluid Mech. (2010), *vol.* 665, *pp.* 516–539.
doi:10.1017/S0022112010004313

The phase lead of shear stress in shallow-water flow over a perturbed bottom

PAOLO LUCHINI[1]† AND FRANÇOIS CHARRU[2]

[1]Dipartimento di Ingegneria Meccanica, Università di Salerno, 84084 Fisciano (SA), Italy

[2]Institut de Mécanique des Fluides de Toulouse, CNRS–Université de Toulouse, 31400 Toulouse, France

(Received 21 February 2010; revised 10 August 2010; accepted 11 August 2010)

The analysis of flow over a slowly perturbed bottom (when perturbations have a typical length scale much larger than channel height) is often based on the shallow-water (or Saint-Venant) equations with the addition of a wall-friction term which is a local function of the mean velocity. By this choice, small sinusoidal disturbances of wall stress and mean velocity are bound to be in phase with each other. In contrast, studies of shorter-scale disturbances have long established that a phase lead develops between wall stress and mean velocity, with a crucial destabilizing effect on sediment transport along an erodible bed. The purpose of this paper is to calculate the wall-shear stress under large length-scale conditions and provide corrections to the Saint-Venant model.

Key words: channel flow, sediment transport, turbulent flows

1. Introduction

The variation of the friction exerted by a fluid flow over a wavy boundary is an important issue in fluid dynamics, e.g. for predicting the pressure loss in pipes or ducts with variable cross-section, or the free-surface level in open flows, or the momentum transfer and wave growth on a deformable interface or the erosion rate on an erodible bed.

In some situations, such as atmospheric flows over hills or water waves, the vertical extent of the flow is so large that it plays no significant role, and the flow may be considered as unbounded, with possibly a boundary-layer structure for the incoming flow. A laminar-flow analysis of such a situation was provided by Benjamin (1959), within the frame of the Orr–Sommerfeld equation in a curvilinear system of coordinates. The analysis is based on the existence of a two-layer structure for the disturbances, namely an inviscid outer layer and a viscous inner layer close to the wavy bottom. The analysis of turbulent flow by Jackson & Hunt (1975) is based on the existence of a similar two-layer structure, with an outer inviscid layer, where advection dominates, and an inner layer where Reynolds stresses play a significant dynamic role and can be modelled using a mixing length. Improvements have been provided by further analyses, see Belcher & Hunt (1998) for a review. For both laminar and turbulent flow, an important result is that the phase of the shear stress leads that of the wavy bottom, owing to the fluid's inertia.

† Email address for correspondence: luchini@unisa.it

Laminar flow	$(h/L)Re \ll 1$	$(h/L)Re \gg 1$
Turbulent flow	$(h/L)c_f^{-1/2} \ll 1$	$(h/L)c_f^{-1/2} \gg 1$
$Re \ll 1$	Very viscous flow (lubrication, falling films)	–
$Re \gg 1$	Fully developed flow	Layered flow
$c_f^{1/2} \ll 1$	(rivers, channels)	(wind over hills or water waves)

TABLE 1. A tentative classification of slowly varying flows ($h/L \ll 1$) and corresponding typical applications (note that the dashed-out case shown with a dash corresponds to requirements which cannot be met together).

On the contrary, for rivers and open channels, or tides in shallow seas, the flow is generally fully developed over its total depth, so that the latter becomes a relevant length scale of the problem. Such flows have been much studied in relation with, in particular, the issues of sediment transport and ripple and dune formation, see Engelund & Fredsoe (1982) for a review. Numerical results have been provided for particular cases, within the framework of some turbulence model (Richards 1980; Sumer & Bakioglu 1984; Colombini 2004). These results show that the shear stress leads the bottom deformation. However, no general relationship was provided. No measurements are available for fully developed flow either: those of Abrams & Hanratty (1985), of the shear stress over a rigid wavy bottom, correspond to a wavelength equal to the channel height, so that the condition for fully developed flow (see below and table 1) is not satisfied.

It seems that a theoretical analysis of bounded fully developed flow is still missing, unlike the case of unbounded flow. One consequence is that the widely used Saint-Venant – depth-averaged – equations still rely on disputable closure laws, for both the shape of the velocity profile and the bottom shear stress, of heuristic or empirical nature (e.g. Balmforth & Mandre 2004).

The goal of this paper is to improve this situation by providing consistent corrections to the bottom shear stress and pressure gradient associated with slow changes in the water depth, for two-dimensional turbulent flow. For such flow, the transverse velocity, normal to the boundary, is much smaller than the characteristic streamwise velocity, U, so that the flow is described by the boundary-layer equations. These equations describe a variety of flows – not only boundary layers – which can be tentatively classified into three types, as presented in table 1. The simplest type corresponds to flows with thickness h not only much smaller than the characteristic length L over which h varies, but also smaller than the viscous diffusion length ν/U: these low-Reynolds-number flows are described by lubrication theory (Batchelor 1967), including, if needed, corrections related to small inertia effects (Chang & Demekhin 2002; Luchini & Charru 2010). Analysis of large-Reynolds-number flows requires a further distinction: whether the flow is fully developed, or not, over the total depth h. The condition for fully developed flow is that the diffusion time of bottom disturbances over the flow depth h is much shorter than the advection time L/U. This diffusion time is h^2/ν for laminar flow, and h/u_τ for turbulent flow where u_τ is the friction velocity, so that the condition for fully developed flow is $(h/L)Re \ll 1$ in the former case, and $(h/L)c_f^{-1/2} \ll 1$ in the latter where c_f is the friction coefficient. If one of these conditions is not met, then the perturbed flow has a layered structure (of two or more layers) as analysed by Belcher & Hunt (1998).

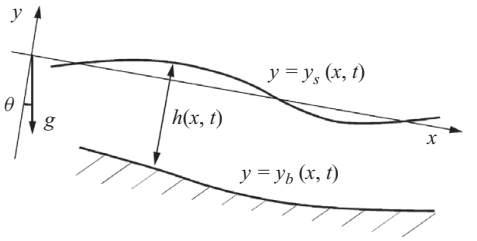

FIGURE 1. Sketch of the free-surface channel with a variable bottom.

The calculation of the inertial correction to the bottom shear stress presented below, and the associated correction to the pressure gradient, will allow the derivation of a consistent set of depth-integrated equations of motion, which replace the classical Saint-Venant equations.

The paper is organized as follows. In § 2, we start by showing the equivalence of flow between a variable bottom and a variable free surface to one in which only the bottom varies and the free surface is replaced by a stress-free symmetry plane. In the next two sections, we solve this problem by a multiple-scale expansion up to first order in the small time-derivative and gradient of the channel depth, first for laminar and then for turbulent flow. In doing so, we derive the quasi-one-dimensional depth-averaged equations that couple the depth to the mean velocity and pressure, and obtain the phase lead of the wall shear stress. Applications will then be presented in § 5 that concern the behaviour of surface waves and the bottom shear stress.

2. Boundary-layer equations for channel flow

We want to address the general problem of free-surface flow driven by gravity on a variable bottom $y_b(x,t)$, when both the free surface and the bottom are slowly varying with x and t except for a constant slope angle θ between the y-axis and gravity (figure 1). The origin of coordinates is at the reference free surface and the y-axis is directed orthogonal to it and upwards (see figure 1), so that the free surface is located at $y = y_s(x,t)$ and the bottom is at $y = y_b(x,t)$ (a negative value). y_s and y_b denote the upward elevations of free surface and bottom, respectively. The local fluid depth is $h(x,t) = y_s(x,t) - y_b(x,t)$.

Whenever the typical scale of variation in the x-direction is asymptotically large compared to the y-scale, the Navier–Stokes equations of either laminar or turbulent incompressible flow reduce to Prandtl's boundary-layer equations, namely in dimensional form

$$u_x + v_y = 0, \quad P_y = 0, \tag{2.1a}$$

$$u_t + uu_x + vu_y + \rho^{-1}P_x = \rho^{-1}\tau_y. \tag{2.1b}$$

Here u and v denote as usual the x- and y-component of velocity. The *modified pressure* P incorporates the effect of gravity g and of the permanent slope θ as

$$P = p + \rho g(y\cos\theta - x\sin\theta), \tag{2.2}$$

where p is the standard thermodynamic pressure. The shear stress τ has been left unspecified so that (2.1*a*, *b*) may equivalently be applied to either laminar or the Reynolds-averaged component of turbulent flow by just inserting a suitable expression for it.

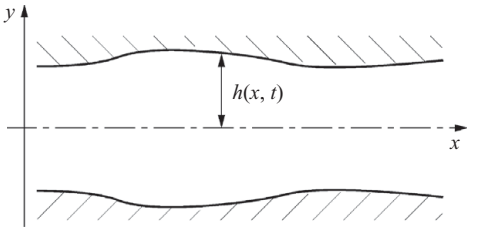

FIGURE 2. Sketch of the symmetric-duct problem, equivalent after the Prandtl transformation to the more general problem of figure 1.

A distinction is needed between the boundary-layer *equations* and the presence of an actual *layer* within the flow space. Equations (2.1*a*,*b*) not only hold in the classical boundary layer, where the x-scale is fixed by the geometry of the solid wall and the y-scale is implicitly determined to be small by the properties of the flow, but also in a channel when the y-scale is given *a priori* but the x- and t-scales turn out to be large. The main difference between these two problems lies in the boundary conditions. In fact, in a classical boundary layer the pressure gradient is imposed by the outer stream and (2.1*a*,*b*) allow only two velocity conditions at the wall and one at infinity, whereas in a duct or channel P_x acts as an additional unknown and the velocity boundary conditions become four. (This is, for instance, the standard procedure used to study the inflow transient.) With reference to figure 1, the boundary conditions are

$$u_y(x, y_s, t) = 0, \quad v(x, y_s, t) = y_{s,t} + u(x, y_s, t)y_{s,x}, \tag{2.3a}$$

$$u(x, y_b, t) = 0, \quad v(x, y_b, t) = y_{b,t}. \tag{2.3b}$$

(More general adherence conditions for a solid moving boundary could be $u(x, y_b, t) = u_b$ and $v(x, y_b, t) = y_{b,t} + u_b y_{b,x}$, where u_b is the horizontal velocity of the bottom. Here we assume our reference frame to be such that the mean horizontal velocity of the bottom is zero, and any variable horizontal velocity that may be caused by deformation to be of higher than the first order in the boundary-layer expansion.)

Within the context of the boundary-layer formulation, the general problem defined above can easily be reduced to the simpler problem of two-dimensional flow between a symmetry (stress-free) plane at $y = 0$ and a single slowly varying wall located at $y = -h(x, t) = y_b - y_s$ (figure 2). Indeed, the boundary-layer equations are known to be invariant under Prandtl's shift (y', v' and y, v denote the old and the new variables, respectively):

$$y = y' - y_s(x, t); \quad v = v' - y_{s,t} - u\, y_{s,x}. \tag{2.4}$$

It can be easily verified that applying (2.4) transforms the boundary conditions (2.3) into

$$u_y(x, 0, t) = v(x, 0, t) = u(x, -h, t) = 0; \quad v(x, -h, t) = -h_t. \tag{2.5}$$

Therefore, the problem of figure 1 is integrally transformed into that of figure 2, and all results obtained for the latter shall be subsequently transferable to the former more general problem using (2.4).

3. Laminar flow in a slowly varying duct

As a preparation for the subsequent analysis of turbulent flow, let us start by examining the laminar solution to the problem defined by (2.1*a*,*b*) with boundary conditions (2.5). We shall do so by two different methods, a straightforward

perturbative expansion of the velocity profile and the consistent section-averaged equations recently introduced by Luchini & Charru (2010).

Depth $h(x,t)$ is assumed to be a given slowly varying function of both variables, such that h_t and h_x are inversely proportional to a large characteristic scale that may asymptotically be driven to infinity. (The total variation in h itself need not be small, only to occur over a large time and distance.) Note that in this analysis the x-scale is not fixed by Reynolds number but rather by the variation of h; thus our results, though based upon the boundary-layer equations, will be uniformly valid with respect to Reynolds number.

At order 0 with respect to h_t and h_x, the continuity equation (2.1a) trivially produces $v^{(0)} = 0$ while the momentum equation (2.1b), with a constant viscosity ν such that $\tau = \rho\nu u_y$, reduces to

$$\nu u^{(0)}_{yy} = \rho^{-1} P^{(0)}_x. \tag{3.1}$$

Its solution is Poiseuille flow:

$$u^{(0)} = (1 - z^2)u_M, \tag{3.2a}$$

$$P^{(0)}_x = \frac{-2\rho\nu u_M}{h^2}, \tag{3.2b}$$

where $z = y/h(x,t)$, $v^{(0)} = 0$, and u_M is the local maximum velocity (attained at $z = 0$).

3.1. *The first-order velocity profile*

At order 1, (2.1a) and (2.1b) become

$$u^{(0)}_x + v^{(1)}_y = 0; \quad P^{(1)}_y = 0, \tag{3.3a}$$

$$\nu u^{(1)}_{yy} - \rho^{-1} P^{(1)}_x = u^{(0)}_t + u^{(0)}u^{(0)}_x + v^{(1)}u^{(0)}_y = u^{(0)}_t + u^{(0)}u^{(0)}_x - u^{(0)}_y \int_0^y u^{(0)}_x \,\mathrm{d}y, \tag{3.3b}$$

with $u^{(1)}_y(0) = u^{(1)}(-h) = v^{(1)}(0) = 0$ and $v^{(1)}(-h) = -h_t$. The latter requires

$$\frac{\partial}{\partial x}\int_{-h}^{0} u^{(0)} \,\mathrm{d}y = Q_x = -h_t, \tag{3.4}$$

where Q is the flow rate per unit width. Equation (3.4) effectively represents a compatibility condition for the two boundary conditions on $v^{(1)}$. It may also be reformulated in terms of the mean velocity $U = Q/h = 2u_M/3$ as

$$h_t + (Uh)_x = 0 \tag{3.5}$$

and is easily recognized to represent the integral form of mass conservation. Equation (3.5) eventually determines the variation of U for a given $h(x,t)$ and then, through (3.2b), the pressure gradient $P^{(0)}_x$. A similar compatibility condition for $v^{(2)}$ requires the integral of $u^{(1)}$ to be constant and implicitly determines the value of the pressure gradient $P^{(1)}_x$. Without loss of generality this constant can be assumed to be zero, so that the zeroth-order flow rate equals the total flow rate, i.e.

$$\int_{-h}^{0} u^{(1)} \,\mathrm{d}y = 0. \tag{3.6}$$

We now change independent variable from y to $z = y/h(x,t)$. By a standard transformation which also finds its use in connection with similarity solutions of the

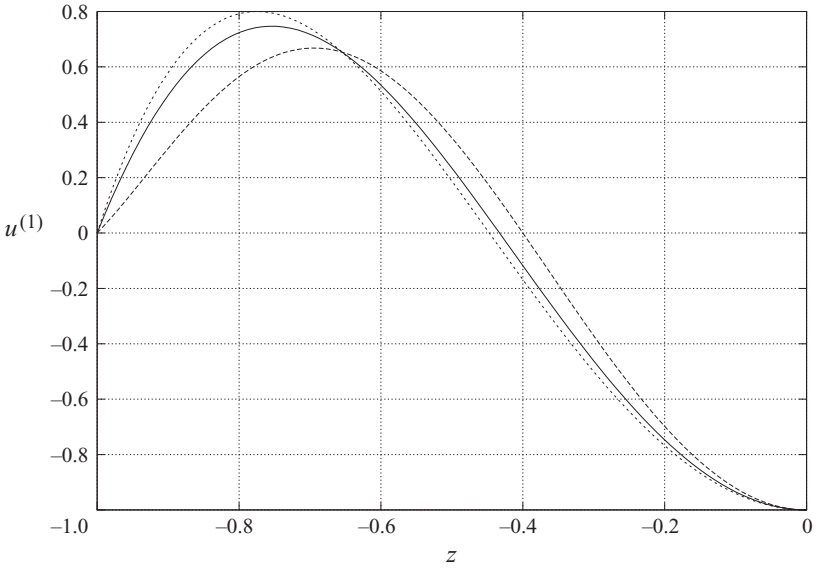

FIGURE 3. First-order velocity correction (3.10): —, coefficient of $u_{M,x}$; – –, coefficient of h_t; - - -, coefficient of $u_{M,t}$.

boundary-layer equations, the right-hand side of (3.3*b*) becomes

$$u_t^{(0)}|_y + u^{(0)}u_x^{(0)}|_y - u_y^{(0)}\int_0^y u_x^{(0)}|_y \,\mathrm{d}y \\ = u_t^{(0)}|_z + u^{(0)}u_x^{(0)}|_z - u_z^{(0)}\int_0^z \left(h_t/h + u_x^{(0)}|_z + h_x u^{(0)}/h\right)\mathrm{d}z. \quad (3.7)$$

It follows from (3.2*a*) and (3.4) that $u_x^{(0)}|_z + h_x u^{(0)}/h = -3(1-z^2)h_t/2h$. Therefore,

$$\nu u_{zz}^{(1)} - h^2\rho^{-1}P_x^{(1)} = h^2 u_{M,t}(1-z^2) + h^2 u_M u_{M,x}(z^4 - 2z^2 + 1) + u_M h h_t(z^4 - z^2). \quad (3.8)$$

Upon integrating twice, the expression of $u^{(1)}$ is found to be

$$\nu u^{(1)} = -h^2 u_{M,t}\, z^4/12 + h^2 u_M u_{M,x}(z^6/30 - z^4/6) \\ + u_M h h_t(z^6/30 - z^4/12) + C_1 z^2 + C_2 z + C_3, \quad (3.9)$$

where C_1, C_2 and C_3 are free constants, with $C_1 = h^2(\rho^{-1}P_x^{(1)} + u_{M,t} + u_M u_{M,x})/2$. Imposing the three conditions $u_z^{(1)}(0) = u^{(1)}(-1) = \int_{-1}^0 u^{(1)}\,\mathrm{d}z = 0$ finally gives

$$\nu u^{(1)} = h^2 u_{M,t}(-z^4/12 + z^2/10 - 1/60) \\ + h^2 u_M u_{M,x}(z^6/30 - z^4/6 + 11z^2/70 - 1/42) \\ + u_M h h_t(z^6/30 - z^4/12 + 2z^2/35 - 1/140) \quad (3.10)$$

with

$$\rho^{-1}P_x^{(1)} = (4/35)u_M h_t/h - (4/5)u_{M,t} - (24/35)u_M u_{M,x}. \quad (3.11)$$

The resulting profiles of the three functions that appear in the expression of the first-order velocity $u^{(1)}(z)$, normalized so that their value at 0 is -1, are shown in

figure 3. Notice that by use of the continuity equation (3.5), (3.10) and (3.11) can be recast as a linear combination of $u_{M,t}$ and any two of h_t, h_x and $u_{M,x}$.

3.2. *Boundary forces*

The first-order solution of (3.3*a*,*b*), in addition to the velocity profile, yields corresponding corrections to both pressure and shear stress at the wall (pressure being important for the evolution of the free surface, if any, and shear stress for its effects on a channel's bottom, as will be exemplified in § 5). The pressure correction was determined by choosing the free constants in the expression of velocity in such a way as to enforce (3.6); by summing together the zeroth-order and first-order results (3.2*b*) and (3.11), while at the same time expressing u_M through the mean velocity $U = 2u_M/3$, the equation providing the total pressure gradient may be rewritten in the following form that will be useful later:

$$\frac{6}{5}U_t + \frac{54}{35}UU_x - \frac{6}{35}\frac{Uh_t}{h} + \frac{P_x}{\rho} = -\frac{3\nu U}{h^2}. \tag{3.12}$$

The first-order shear stress $\tau_w^{(1)}$ at the boundary $y = -h(x,t)$, on the other hand, is proportional to the derivative of the velocity correction (3.10), and allows the total shear stress to be expressed as

$$\tau_w = \tau_w^{(0)} + \tau_w^{(1)} = \frac{3\rho\nu U}{h}\left(1 + \frac{h^2U_t}{15\nu U} + \frac{4h^2U_x}{35\nu} + \frac{hh_t}{105\nu}\right). \tag{3.13}$$

In steady flow (where $hU = $ const. and thus $hU_x = -Uh_x$), this expression simplifies to

$$\tau_w = [1 - (4Re/35)h_x]\,\tau_w^{(0)}, \tag{3.14}$$

where $Re = hU/\nu$ is the mean-velocity Reynolds number and is, in this particular case, constant with x.

It should be remarked that for undulating height perturbations, the term proportional to h_x is in quadrature with h itself, whereas the zeroth-order shear stress (which changes quasi-statically, insofar as it is proportional to $U/h = Q/h^2$) is in phase with it. Signs are such that the first-order correction produces a *phase lead*.

3.3. *The method of consistent section-averaged equations*

If only the boundary forces are of interest and not the details of the velocity profile, a quicker way to obtain the former directly was proposed by Luchini & Charru (2010). In view of a subsequent generalization to turbulent flow in the next section, it may be interesting now to verify that the laminar pressure gradient and shear stress can indeed be re-obtained in this way.

The key observation is that an equation such as (3.12), tying the mean velocity to the first-order-corrected pressure gradient, can be consistently generated from the integrated form of the kinetic-energy balance (Bernoulli) equation, while only using the zeroth-order velocity profile. (The kinetic-energy equation had already been noted by Usha & Uma (2004) to give the right stability threshold of long waves in a falling liquid film, but its generality as a consistent nonlinear formulation does not appear to have been recognized at the time.)

The kinetic-energy balance appropriate to the boundary-layer approximation can be constructed by multiplying (2.1*b*) by u and integrating, which can be written as

$$\frac{\partial}{\partial t}\frac{\alpha hU^2}{2} + \frac{\partial}{\partial x}\frac{\beta hU^3}{2} + \frac{hUP_x}{\rho} = -f^{(0)}, \tag{3.15}$$

where $f^{(0)}$ is the dissipation function, $f^{(0)} = \nu \int_{-h}^{0} u_y^{(0)2}\,\mathrm{d}y$ (the index (0) emphasizing that it is evaluated for the zeroth-order velocity profile), and α and β are the form factors

$$\alpha = \frac{1}{hU^2}\int_{-h}^{0} u^{(0)2}\,\mathrm{d}y, \quad \beta = \frac{1}{hU^3}\int_{-h}^{0} u^{(0)3}\,\mathrm{d}y. \tag{3.16}$$

The reason (3.15) holds true for the first-order-accurate pressure gradient is that the first two terms, containing time- and x-derivatives, are already of first order while the dissipation, owing to the minimum-dissipation property of laminar flow in a straight channel, has a vanishing first-order correction (Luchini & Charru 2010).

In order to be compared to the outcome of the previous section, (3.15) can be transformed to a convective form, by subtracting the continuity equation multiplied by $\beta U^2/2$ and then dividing by h. It results in

$$\frac{\partial}{\partial t}\frac{\alpha U^2}{2} + U\frac{\partial}{\partial x}\frac{\beta U^2}{2} - (\beta-\alpha)\frac{U^2}{2h}\frac{\partial h}{\partial t} + \frac{U P_x}{\rho} = -\frac{f^{(0)}}{h}. \tag{3.17}$$

For the parabolic laminar velocity profile, the coefficients (3.16) and the dissipation function, respectively, are evaluated as $\alpha = 6/5$, $\beta = 54/35$ and $f^{(0)} = 3\nu U^2/h$. With these values, (3.17) can be recognized to be term-by-term identical to (3.12). Yet the first-order velocity correction $u^{(1)}$ was not involved in its derivation this time.

After the pressure gradient P_x has been determined to first order, in one or the other way, the section-averaged momentum equation becomes instrumental in calculating the first-order-accurate wall-shear stress τ_w. The integral of (2.1*b*) from $-h$ to 0 may be written as

$$(hU)_t + (\alpha h U^2)_x + h\rho^{-1}P_x = -\rho^{-1}\tau_w, \tag{3.18}$$

where $\tau_w(x,t)$ is the fluid shear stress on the bottom surface and α is the same form factor already defined in (3.16). Differently from the dissipation function, τ_w contains both zeroth- and first-order contributions, and cannot be considered known *a priori*. However, P_x has already been extracted from either (3.12) or (3.17) and is now known; the momentum integral then becomes an expression for τ_w itself.

The convective form of (3.18), obtained by subtracting the continuity equation multiplied by αU and then dividing by h, reads

$$-\frac{\tau_w}{\rho h} = U_t + U(\alpha U)_x - (\alpha-1)\frac{U h_t}{h} + \frac{P_x}{\rho}. \tag{3.19}$$

For $\alpha = 6/5$, eliminating P_x between (3.19) and (3.17) exactly reproduces the shear stress previously obtained in (3.13), a result which can also be easily verified.

4. Turbulent flow

Under turbulent-flow conditions, the Reynolds-averaged turbulent velocity is still governed by (2.1) with boundary conditions (2.5). The closure of these equations, however, requires a *turbulence model* for the shear stress, τ.

4.1. *Constant-viscosity turbulence model*

The simplest possible turbulence model is a constant eddy viscosity. Although this is a very rough model and is likely to be insufficient for most applications, here we consider it first, for the two reasons that its use is not rare in connection with shallow-water flow (Engelund 1970) and that it may serve as a comparison baseline for subsequent improvement.

The justification for an eddy viscosity being held constant is that all models that use a variable one predict negligible variations in the central part of a channel. Adopting a constant eddy viscosity everywhere amounts to supposing that only the central region is important for the phenomenon under study. Of course, already a sign of the dangers of this assumption is that the mean turbulent flow in a straight channel then turns out to have a parabolic Poiseuille profile just like a laminar flow. This is contrasted by the obvious advantage that one can immediately recycle all laminar results by simply inserting an appropriate value of viscosity in them. It seems fair to determine this effective (turbulent + laminar) viscosity by imposing that at zeroth order it should return the empirically observed friction coefficient $c_f = 2\tau_w^{(0)}/\rho U^2$. The effective viscosity having this property is

$$\nu = \frac{c_f h U}{6}. \tag{4.1}$$

In turbulent flow, c_f may generally be a function of Reynolds number as well as wall roughness; by parameterizing our results in c_f we implicitly account for an arbitrary dependence on both. With this choice (3.13) and (3.14), respectively, become

$$\tau_w = \left(c_f + \frac{2}{5}\frac{hU_t}{U^2} + \frac{24}{35}\frac{hU_x}{U} + \frac{2}{35}\frac{h_t}{U}\right)\frac{\rho U^2}{2} \quad \text{(unsteady)}, \tag{4.2}$$

$$\tau_w = [c_f - (24/35)h_x]\rho U^2/2 \quad \text{(steady flow)}. \tag{4.3}$$

4.2. *Variable-viscosity turbulence model*

The main defect of assuming a constant eddy viscosity, to predict an unrealistic mean-velocity profile, may be overcome by adopting a variable eddy viscosity which depends on the wall-normal coordinate y (an algebraic turbulent-viscosity model, as it is commonly qualified to distinguish it from those that introduce additional differential equations). In fact, replacing (3.1) by

$$\left[\nu(y)u_y^{(0)}\right]_y = \rho^{-1}P_x^{(0)} \tag{4.4}$$

can return just any desired mean-velocity profile $u^{(0)}(y)$ provided only

$$\nu(y) = \frac{\tau^{(0)}}{\rho u_y^{(0)}} = \frac{yP_x^{(0)}}{\rho u_y^{(0)}} = \frac{-y\tau_w^{(0)}}{\rho h u_y^{(0)}}. \tag{4.5}$$

The unperturbed velocity profile then becomes the starting point of the analysis. Equation (4.5) was repeatedly exploited in the past to deduce a turbulent-viscosity diagram from analytical (Hinze 1975), experimental (Nezu & Rodi 1986) or numerical (Jimenez *et al.* 2001) mean-flow velocity data. The underlying closure assumption (the 'model') is then that the same effective viscosity as obtained from (4.5) will govern velocity perturbations. This is not necessarily granted but, since it is not the purpose of this paper to delve into the intricacies of turbulence modelling, we restrict ourselves to saying that our results will be valid within the limitations of an algebraic turbulence model, with all the reservations that the eddy-viscosity concept itself requires. It is, at any rate, the same assumption as in Jackson & Hunt (1975) and a vast improvement over a constant viscosity.

An algebraic turbulent-viscosity model has the very useful property that (4.4) is still endowed with a minimum-dissipation property just as when viscosity is constant. Therefore, the consistent section-averaged formulation of § 3.3 remains valid. We shall now pursue this quicker approach, deferring the calculation of the velocity perturbation to the Appendix.

Multiplying (4.4) by $u^{(0)}$ and integrating by parts gives

$$hU\rho^{-1}P_x^{(0)} = -\int_{-h}^{0} \nu(y)u_y^{(0)2}\,\mathrm{d}y = -f^{(0)}. \tag{4.6}$$

Conversely, nullifying the first variation of $f^{(0)}$ under the constraint of an unchanging flow rate gives back (4.4). On the other hand, integrating (4.4) itself from $-h$ to 0 yields $hP_x^{(0)} = -\rho\nu(-h)u_y^{(0)}(-h) = -\tau_w^{(0)}$. Comparing these two expressions of $P_x^{(0)}$, we can write the zeroth-order dissipation function simply as

$$f^{(0)} = \rho^{-1}U\tau_w^{(0)} = \frac{c_f U^3}{2} \tag{4.7}$$

(just another form of the law of energy conservation). The kinetic-energy balance equation (3.17) then applies unchanged to turbulent flow, provided only the α and β coefficients are properly recalculated according to (3.16) from the new velocity profile, and directly yields an expression for the first-order-accurate pressure gradient P_x. Remarkably, the turbulent eddy viscosity does not explicitly appear in it.

The expression of the first-order shear-stress correction, on the other hand, is generated just as in laminar flow, by taking the difference between the kinetic-energy equation (3.17) divided by U and the momentum equation (3.19), namely:

$$\frac{\tau_w^{(1)}}{\rho h} = \frac{1}{U}\frac{\partial}{\partial t}\frac{(\alpha-1)U^2}{2} + \frac{\partial}{\partial x}\frac{(\beta-\alpha)U^2}{2} - \frac{U^2}{2}\frac{\partial\alpha}{\partial x} - (\beta-3\alpha+2)\frac{U}{2h}\frac{\partial h}{\partial t}. \tag{4.8}$$

By just assuming that an algebraic turbulent eddy viscosity exists, but without actually using its expression, the consistent section-averaged formulation thus allows us to cast the first-order wall-shear correction in a form that depends only on the α and β coefficients and ultimately on the shape of the turbulent mean-velocity profile. It is true that an equivalent viscosity is uniquely specified by the velocity profile through (4.5), but its elimination is nonetheless important because (4.5) contains the derivative of velocity while (4.8) contains only its integrals, and is thus much more robust in the face of possible imprecisions in the profile itself. The form of (4.8), in addition, elucidates that the wall-shear correction actually depends on the departure of α and β from unity, that is of the velocity profile from flatness. As a turbulent profile is typically flatter than a parabola, we can already suspect that the constant-viscosity assumption of §4.1, with its ensuing parabolic velocity profile, is likely to have overestimated the shear stress.

4.3. *Wall layer and defect layer*

In order to evaluate the α and β integrals and thus obtain an explicit expression for the boundary forces, we shall now introduce the standard asymptotic separation of the turbulent flow into a wall layer and a defect layer. Let us stress, however, that this is not an obligatory step: these form factors only depend on the unperturbed velocity profile in a straight duct. They can be more accurately generated if needed, for instance by integrating an experimental or a numerical velocity profile.

The distinctively most successful description of wall-bounded turbulent flow is its conceptual separation into two regions: a *wall layer*, where velocities are of the order of the wall-shear velocity u_τ (defined as $u_\tau = \sqrt{\tau_w/\rho}$) and distance from the wall is of the order of ν/u_τ, and a *defect layer* where the velocity defect $u_M - u$ (u_M being the maximum of u) is of the order of u_τ and distances span most of the height h. The two overlap in a *logarithmic region* where velocity u increases from $O(u_\tau)$ to $u_M - O(u_\tau)$ like $u_\tau\kappa^{-1}\log(h+y) + \text{const.}$, κ being the von Kármán's constant. The separation

between wall and defect layer becomes more and more pronounced as $u_\tau/u_M \to 0$, and in this sense u_τ/u_M (or equivalently u_τ/U) may be regarded as the small parameter around which asymptotic descriptions of turbulent flow are built. Since $u_\tau/U = (c_f/2)^{1/2}$ turns out to be approximately proportional to $[\log(Re_\tau)]^{-1}$, where $Re_\tau = hu_\tau/\nu$, it can be maintained that asymptotic theories of turbulent flow are expansions in powers of the square root of the friction coefficient, or equivalently of the reciprocal logarithm of Reynolds number (Mellor 1972). (Incidentally, we may remark that such an expansion introduces an additional small parameter in the analysis, independent of the typical time and length scales characterizing the boundary oscillations.)

The wall layer gives a negligible contribution (an exponentially small one in the parameter u_τ/U) to the integrals in (3.16); therefore to evaluate α and β we only need the properties of the defect layer, where the zeroth-order velocity profile is known to have the functional dependence

$$u^{(0)} = u_M + u_\tau F(y/h). \tag{4.9}$$

The universal dimensionless function $F(y/h)$ can be obtained from a theory, an experiment or a numerical simulation, but its only independent variable is the dimensionless coordinate $z = y/h$. In particular, it is independent of the physical viscosity and/or wall roughness, which only appear in (4.9) by indirectly affecting the value of u_τ. In the matching region with the wall layer, $z \to -1$, the velocity profile must behave logarithmically as $u \sim u_\tau \kappa^{-1} \log(1+z) + \text{const}$. A very common assumption for channel flow is just to extend this logarithmic behaviour all the way to the free surface $z = 0$, thus writing $F(z) = \kappa^{-1}\log(1+z)$ and

$$u^{(0)} = u_M + \kappa^{-1} u_\tau \log(1+z). \tag{4.10}$$

This is because the departure from logarithmic behaviour, the so-called wake region, is in this case rather small (Nezu & Rodi 1986). On the wall side (4.10) diverges but its integral converges. In order to obtain a simple closed-form result, we shall now calculate the first-order shear-stress correction using (4.10).

The first step is to express the maximum through the mean velocity. From the integral of (4.10):

$$U = \frac{Q}{h} = u_M + \frac{u_\tau}{\kappa}\int_{-1}^{0} \log(1+z)\,\mathrm{d}z = u_M - \frac{u_\tau}{\kappa}, \tag{4.11}$$

whence

$$u^{(0)} = U + \kappa^{-1} u_\tau [1 + \log(1+z)]. \tag{4.12}$$

The coefficients we need, defined in (3.16), are then

$$\alpha - 1 = \left(\frac{u_\tau}{\kappa U}\right)^2 \int_{-1}^{0} [1+\log(1+z)]^2\,\mathrm{d}z = \left(\frac{u_\tau}{\kappa U}\right)^2, \tag{4.13a}$$

$$\begin{aligned}\beta - 1 &= 3\left(\frac{u_\tau}{\kappa U}\right)^2 \int_{-1}^{0} [1+\log(1+z)]^2\,\mathrm{d}z + \left(\frac{u_\tau}{\kappa U}\right)^3 \int_{-1}^{0} [1+\log(1+z)]^3\,\mathrm{d}z \\ &= 3\left(\frac{u_\tau}{\kappa U}\right)^2 - 2\left(\frac{u_\tau}{\kappa U}\right)^3.\end{aligned} \tag{4.13b}$$

Since the separation between wall layer and defect layer is in fact an expansion in powers of u_τ/U, the term in $(u_\tau/U)^3$ can be neglected as compared to $(u_\tau/U)^2$. Recalling that $(u_\tau/U)^2 = c_f/2$, it turns out that the spatial and temporal derivatives of α and β, though non-zero in turbulent flow, are $O[(u_\tau/U)^3]$ and thus negligible.

As a consequence, the total wall-shear stress expressed by (4.8) can be given by

$$\tau_w = \tau_w^{(0)} + \tau_w^{(1)} = \left(1 + \frac{1}{\kappa^2}\frac{hU_t}{U^2} + \frac{2}{\kappa^2}\frac{hU_x}{U}\right) c_f \frac{\rho U^2}{2}, \tag{4.14}$$

or for steady flow (where $hU = \text{const.}$) by

$$\tau_w = \left(1 - \frac{2}{\kappa^2} h_x\right) c_f \frac{\rho U^2}{2}. \tag{4.15}$$

This is our main result. In turbulent, as in laminar, flow on an undulated surface the first-order correction to wall shear entails a phase lead. As in § 4.1, the dependence of (4.14)–(4.15) upon the Reynolds number and wall roughness has been encapsulated in the unperturbed friction coefficient c_f. Notice also that in the limit of $c_f \to 0$ (which is formally achieved, though logarithmically slowly, when $Re \to \infty$ on a smooth surface) the whole shear stress goes to zero but the ratio between the first- and zeroth-order terms (and thus the phase lead) remains proportional to h_x. For a sinusoidal disturbance of wavenumber k and for constant c_f, the phase angle is precisely kh/κ^2 (but see (5.14*b*) below for the effect of a variable c_f).

Finally, it must be remarked that the correction (4.3) provided by the constant-viscosity turbulence model was larger than the correction obtained for τ_w in (4.15) by a factor $\approx 0.05 c_f^{-1}$ (e.g. by five times for $c_f = 0.01$). Any suspicions that the constant-viscosity model might be inadequate are thus confirmed.

5. Applications

In this section we revisit three classical problems treated within the framework of the shallow-water equations, and show how their results are modified by the first-order consistent formulation. These problems are surface-wave propagation and its characteristic lines, the stability of a free-surface flow over a flat bottom, and the steady free-surface flow over a wavy bottom.

5.1. *Classical versus consistent formulation of the quasi-one-dimensional channel problem*

We now return to the general problem of channel flow between a variable bottom at the position $y = y_b(x,t)$ and a free surface at the position $y = y_s(x,t) = y_b + h$, the problem that was depicted in figure 1. If interaction with the air above is neglected, pressure p at the position $y = y_s(x,t)$ must be constant. The x-derivative of (2.2) along the surface then gives

$$P_x = \rho g(y_{s,x}\cos\theta - \sin\theta). \tag{5.1a}$$

The classical formulation of this problem (de Saint-Venant 1871) starts from the integral laws of mass and momentum conservation written on the assumption that local velocity is close enough to its mean value to be confused with a plug flow. The following notation is used:

$$h_t + (Uh)_x = 0, \tag{5.1b}$$

$$U_t + UU_x + \rho^{-1}P_x = -h^{-1}\rho^{-1}\tau_w. \tag{5.1c}$$

(Of course, (5.1*c*) may also be seen as a particular case of (3.19) with $\alpha = 1$.) These equations are then combined with an empirical closure for the bottom shear stress. Since first-order corrections play no role in the classical theory, the typically assumed

closure relation for τ_w is the zeroth-order equation

$$\tau_w = \frac{c_f \rho U^2}{2}. \tag{5.1d}$$

Inserting P_x from (5.1a) and τ_w from (5.1d) into (5.1b)–(5.1c), thus leaves a system of two differential equations in the two unknowns h and U.

The Saint-Venant equations (5.1) are widely used for environmental problems in the atmosphere and the ocean, as well as in rivers (Balmforth & Mandre 2004; Pedlosky 2003; Whitham 1974). They also describe gravity currents and snow avalanches (Hopfinger 1983), as well as thin granular flows on slopes (Aradian, Raphael & de Gennes 2002; Forterre & Pouliquen 2008). They also provide a useful model in engineering calculations, e.g. for the pressure drop and phase distribution in two-phase flows in ducts (Lin & Hanratty 1986). However, it should by now be clear that the formulation (5.1) does not contain all the order-one contributions that arise from a consistent account of the deviation of the velocity profile from flatness. Nor is it wholly consistent with a plug-flow limit, which would imply that the whole shear stress (but not its phase lead) becomes zero as compared to the other terms in (5.1c).

A consistent formulation obviating these difficulties, as shown in the previous sections, replaces the pair of equations (5.1c) and (5.1d) by the kinetic-energy equation (3.17), which for the values (4.13b) of the correction coefficients may be written to within an error $O[(u_\tau/U)^3]$ as

$$\left(1+\frac{c_f}{2\kappa^2}\right) U_t + \left(1+\frac{3c_f}{2\kappa^2}\right) U U_x - \frac{c_f}{2\kappa^2}\frac{U h_t}{h} + \frac{P_x}{\rho} = -\,c_f \frac{U^2}{2h}. \tag{5.2a}$$

The wall-shear stress decouples from the system, and the momentum equation is not involved at all in the determination of the pressure gradient. Indeed, its role is reversed with respect to the classical formulation: rather that accepting a heuristically imposed τ_w and providing a pressure gradient P_x to balance gravity in (5.1a), the momentum equation now takes P_x from the solution of the rest of the system and becomes the means by which a first-order accurate τ_w can be calculated. For this purpose, the momentum equation (3.19) with the α coefficient taken from (4.13a) reads

$$-\frac{\tau_w}{\rho h} = U_t + \left(1+\frac{c_f}{2\kappa^2}\right) U U_x - \frac{c_f}{2\kappa^2}\frac{U h_t}{h} + \frac{P_x}{\rho}. \tag{5.2b}$$

Eliminating P_x between (5.2a) and (5.2b) yields the expression of τ_w that was previously shown as (4.14).

5.2. *Base flow and linearized disturbance equations*

A quantitative comparison between the two formulations will now be performed with reference to the problem of small perturbations of a constant base flow. In a straight open-surface channel, the classical formulation (5.1a)–(5.1d) and the consistent formulation composed of (5.1a), (5.1b) and (5.2a) share the following constant base solution for the velocity $U = \bar{U}$ and flow height $h = \bar{h}$:

$$\bar{U}^3 = g\cos\theta\, Fr^2\, Q, \quad \bar{h}^3 = \frac{Q^2}{g\cos\theta\, Fr^2} \tag{5.3}$$

where Q is the flow rate per unit width and Fr is the Froude number defined by

$$Fr^2 = \frac{\bar{U}^2}{g\bar{h}\cos\theta} = \frac{2\tan\theta}{\bar{c}_f}. \tag{5.4}$$

For small perturbations of either the bottom or the free surface, letting $h = \bar{h} + \delta h$, $U = \bar{U} + \delta U$ and linearizing the classical formulation (5.1) yields

$$\delta h_t + \bar{U}\delta h_x + \bar{h}\delta U_x = 0, \tag{5.5a}$$

$$\delta U_t + \bar{U}\,\delta U_x + g\cos\theta\,(\delta y_b + \delta h)_x = -\delta\left(\frac{\tau_w}{\rho h}\right), \tag{5.5b}$$

$$\delta\left(\frac{\tau_w}{\rho h}\right) = \bar{c}_f\frac{\bar{U}^2}{\bar{h}}\left[\frac{\delta U}{\bar{U}} - (1+b)\frac{\delta h}{2\bar{h}}\right]. \tag{5.5c}$$

The term b appearing in the last equation, defined as

$$b = -\frac{\bar{h}}{\bar{c}_f}\frac{\mathrm{d}c_f}{\mathrm{d}h}, \tag{5.6}$$

accounts for the possible dependence of the friction coefficient on depth h in the fully rough regime of turbulent friction. Its value can be obtained from the logarithmic law (A 17), i.e. $b = \kappa^{-1}\sqrt{2\bar{c}_f}$ which gives $b = 0.35$ for $\bar{c}_f = 0.01$. Tangent to (A 17) in this range of c_f is the empirical Manning–Strickler power law $c_f \propto (h/h_r)^{-b}$ with $b = 1/3$, as used for similar purposes by Gradowczyk (1968).

For the same problem, linearizing the consistent equations (5.1*b*) and (5.2*a*) instead gives

$$\delta h_t + \bar{U}\delta h_x + \bar{h}\delta U_x = 0, \tag{5.7a}$$

$$(1 + a\bar{c}_f)\delta U_t + (1 + 3a\bar{c}_f)\bar{U}\delta U_x - a\bar{c}_f\frac{\bar{U}\delta h_t}{\bar{h}} + g\cos\theta\,(\delta y_b + \delta h)_x = -\bar{c}_f\frac{\bar{U}^2}{\bar{h}}\left[\frac{\delta U}{\bar{U}} - (1+b)\frac{\delta h}{2\bar{h}}\right], \tag{5.7b}$$

with the wall-shear stress (4.14) linearized as

$$\frac{\delta\tau_w}{\bar{\tau}_w} = 2\frac{\delta U}{\bar{U}} - b\frac{\delta h}{\bar{h}} + 2a\,\frac{\bar{h}\delta U_t}{\bar{U}^2} + 4a\,\frac{\bar{h}\delta U_x}{\bar{U}}. \tag{5.7c}$$

Here we have introduced

$$a = (2\kappa^2)^{-1}. \tag{5.8}$$

5.3. *Characteristic lines of the shallow-water problem*

The classical shallow-water problem is hyperbolic and admits surface waves with speed $\bar{U} \pm \sqrt{g\bar{h}\cos\theta}$. As is well known, the properties of steady flow are affected by the direction of propagation of such waves, and change when both wave families propagate downstream, that is when the Froude number exceeds unity. This behaviour is modified when the inertial correction to the bottom friction is taken into account. In order to determine the characteristic lines of the system, according to Whitham (1974), we collect coefficients of the first derivatives of the unknowns in the form of a matrix and write the vector equation

$$\begin{pmatrix}\delta h_t\\ \delta U_t\end{pmatrix} + \begin{bmatrix}\bar{U} & \bar{h}\\ \dfrac{g\cos\theta + a\bar{c}_f\bar{U}^2/\bar{h}}{1+a\bar{c}_f} & \dfrac{1+4a\bar{c}_f}{1+a\bar{c}_f}\bar{U}\end{bmatrix}\begin{pmatrix}\delta h_x\\ \delta U_x\end{pmatrix} = \cdots, \tag{5.9}$$

where the right-hand side, not written, involves δh, δU and the prescribed bottom slope $\delta y_{b,x}$. The characteristic lines of this system are determined by the eigenvalues

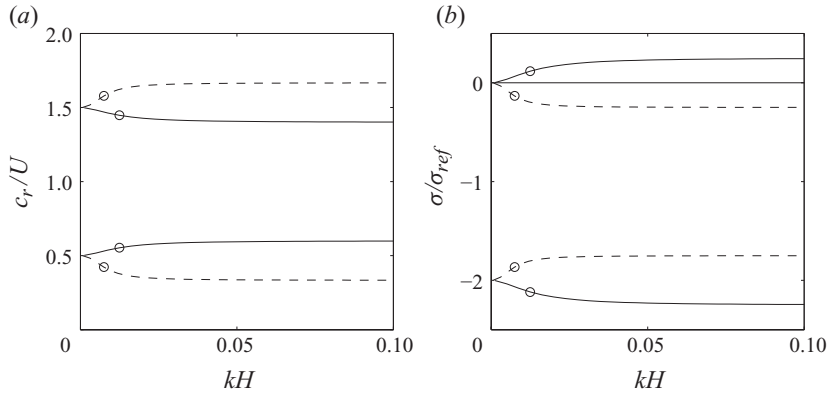

FIGURE 4. Wave velocity (a) and growth rate (b) of the slow and fast modes, for $Fr = 1.5$ (dashed line) and $Fr = 2.5$ (continuous line); circles (○) correspond to $k\bar{h} = \bar{c}_f Fr/2$. $\sigma_{ref} = \bar{c}_f \bar{U}/2\bar{h}$, $\bar{c}_f = 0.01$.

of the matrix of x-derivative coefficients. It can be noticed that setting $a\bar{c}_f = 0$ in (5.9) returns the coefficient matrix of the classical surface-wave problem. From the calculation of the propagation velocity of the characteristic lines, it can be easily shown that both characteristics will propagate downstream when the Froude number exceeds the critical value given by

$$Fr_c^2 = \frac{1}{1 + 3a\bar{c}_f}. \tag{5.10}$$

As an example, for $\bar{c}_f = 0.01$ the critical Froude number becomes 0.96, slightly lower than the value unity of the classical surface-wave problem in shallow waters.

5.4. *Stability of a free-surface flow over a flat bottom*

We now investigate the stability of flow over a flat bottom ($\delta y_b = 0$), as first studied by Jeffreys (1925). The system (5.7a, b) admits sinusoidal solutions, such that $\delta h = \mathrm{Re}(\hat{h}\exp[\mathrm{i}k(x - ct)])$ and $\delta U = \mathrm{Re}(\hat{U}\exp[\mathrm{i}k(x - ct)])$, with the dispersion relation

$$(1 + a\bar{c}_f)\left(\frac{c}{\bar{U}} - 1\right)^2 - a\bar{c}_f\left(3\frac{c}{\bar{U}} - 2\right) - \frac{1}{Fr^2} + \frac{\mathrm{i}\bar{c}_f}{k\bar{h}}\left(\frac{c}{\bar{U}} - \frac{3+b}{2}\right) = 0. \tag{5.11}$$

Setting $a = b = 0$ yields Jeffreys' result. The correction term b, accounting for a variable friction coefficient, was introduced in a similar stability analysis by Gradowczyk (1968), whereas the inertial correction $a\bar{c}_f$ is introduced here for the first time.

Let us first consider the classical formulation (5.5) with $b = 0$, whose dispersion relation equals (5.11) with $a = b = 0$. (As pointed out by Whitham (1974, pp. 85 and 134), this case is actually better analysed through the nonlinear equations and leads to the so-called *roll waves*, as studied, e.g. by Needham & Merkin 1984.) The two roots of the dispersion relation correspond to a wave mode and a damped mode. Figure 4(a) displays the real part of the two modes, for two Froude numbers below and above the neutral-stability Froude number $Fr = 2$. It shows that the velocity tends to $(1 \pm 1/2)\bar{U}$ for vanishing wavenumber and is close to $\bar{U} \pm \sqrt{g\bar{h}\cos\theta}$ for large wavenumber. Figure 4(b) displays the normalized growth rate. The damped mode is strongly so (damping rate larger than frequency) for any wavenumber and Froude number, whereas the wave mode is weakly damped when $Fr < 2$, and unstable for all

wavenumbers when $Fr > 2$. For $k\bar{h} \ll \bar{c}_f Fr/2$ the growth rate σ scales as $(k\bar{h})^2$, and for larger wavenumber it tends to the constant value

$$\sigma = \frac{\bar{c}_f \bar{U}}{2\bar{h}} \left(-1 \pm \frac{Fr}{2} \right). \tag{5.12}$$

On including the two corrections $a\bar{c}_f$ and b, the general picture shown by figure 4 remains the same, but the flow becomes unstable for all wavenumbers at a Froude number Fr_t now given by

$$\frac{1}{Fr_t^2} = \frac{(1+b)^2}{4} - a\bar{c}_f \frac{9 + 4b - b^2}{4}. \tag{5.13}$$

Gradowczyk's b correction decreases the threshold Froude number from Jeffreys' value $Fr_t = 2$, whereas the inertial correction $a\bar{c}_f$ increases it. For example, the b correction alone gives $Fr_t = 1.48$ with $b = 0.35$ (or $Fr_t = 1.5$ with $b = 1/3$), whereas the inertial correction alone gives $Fr_t = 2.36$ with $\bar{c}_f = 0.01$ ($a\bar{c}_f = 0.031$); when both corrections are included, Fr_t turns out to be 1.63.

To date the precise threshold remains open to experimental verification. Whereas nonlinear roll waves at large Froude number have been well investigated (e.g. Brock 1969), no specific study, to our knowledge, reports the experimental determination of the stability threshold. An experimental investigation of the analogous laminar problem (Julien & Hartley 1986) suggests that the threshold may be rather elusive.

5.5. *Steady flow over a wavy bottom*

We now consider linearized stationary flow over a sinusoidal bottom $\delta y_b = \mathrm{Re}(\hat{y}_b \exp[\mathrm{i}kx])$, with small amplitude ($|\hat{y}_b| \ll h$) and zero phase (real $\hat{y}_b$), with particular interest in the phase angle of the disturbance of the bottom shear stress. Indeed, on an erodible bed, the component of the shear-stress disturbance in phase with the ripples is responsible for their migration, whereas the out-of-phase component is responsible for their growth or decay: positive angle corresponds to ripple growth (unstable flat bed) and negative angle to ripple decay (stable flat bed).

For Froude number smaller than the threshold (5.13), we have shown that the flow is stable; in this range, the disturbances induced by the wavy bottom can be calculated from the linearized consistent equations (5.7) with time derivatives set to zero. On introducing $\delta h = \mathrm{Re}(\hat{h} \exp[\mathrm{i}kx])$ and $\delta U = \mathrm{Re}(\hat{U} \exp[\mathrm{i}kx])$, the substitution of (5.7*a*) into (5.7*b*) and (5.7*c*) gives, respectively,

$$\frac{\hat{h}}{\bar{h}} = \left(\frac{Fr^2}{Fr_c^2} - 1 - \mathrm{i}(3+b) \frac{\bar{c}_f Fr^2}{2k\bar{h}} \right)^{-1} \frac{\hat{y}_b}{\bar{h}}, \tag{5.14a}$$

$$\frac{\hat{\tau}_w}{\bar{\tau}_w} = \frac{|\hat{\tau}_w|}{\bar{\tau}_w} \mathrm{e}^{\mathrm{i}\phi} = -(2 + b + 4\mathrm{i}a\,k\bar{h}) \frac{\hat{h}}{\bar{h}}, \tag{5.14b}$$

where the critical Froude number Fr_c turns out to be the same as in (5.10), arising from the analysis of characteristic lines. The first of the above equations gives the disturbance of the local flow depth, and the second then gives the disturbance of the bottom shear stress. Figure 5 displays the modulus and phase of $\hat{\tau}_w$ according to both the classical (dashed lines) and consistent (solid lines) formulations, for the subcritical Froude number $Fr^2 = 0.5\, Fr_c^2$ (figure 5*a*,*b*) and for the supercritical Froude number $Fr^2 = 2\, Fr_c^2$ (figure 5*c*,*d*).

For small wavenumber, $k\bar{h} \ll \bar{c}_f Fr/2$, the disturbance of the flow depth h, just as that of the velocity U, is very small with respect to y_b, i.e. of the order of $\mathrm{i}k\hat{y}_b$. Thus

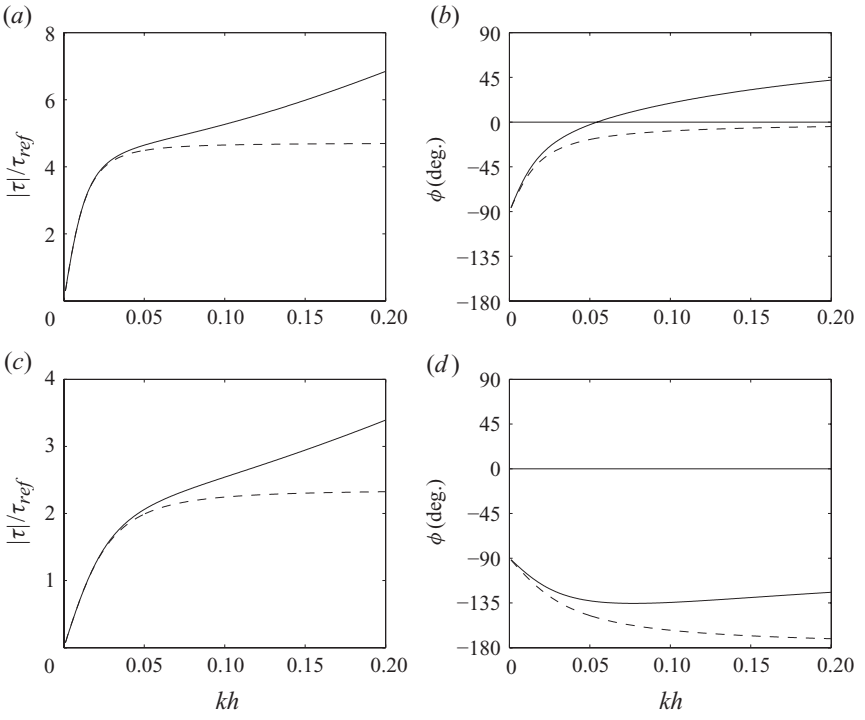

FIGURE 5. Modulus and phase of the bottom shear stress $\tau_w = |\tau_w| e^{i\phi}$ for $a = 0$ (– –) and $a = 1/(2\kappa^2)$ (—). (*a*, *b*), $Fr^2 = 0.5\, Fr_c^2$; (*c*, *d*), $Fr^2 = 2\, Fr_c^2$. $\tau_{ref} = (\hat{y}_b/\bar{h})\bar{\tau}$, $\bar{c}_f = 0.01$, $Fr_c = 0.96$, $b = 0.35$.

the free surface follows the bottom deformation. The perturbation of the bottom shear stress is found from (5.14) to be

$$\frac{\hat{\tau}_w}{\bar{\tau}_w} \sim -2\mathrm{i}\,\frac{2+b}{3+b}\,\frac{k\bar{h}}{\bar{c}_f\, Fr^2}\,\frac{\hat{y}_b}{\bar{h}}, \tag{5.15}$$

with phase angle $\phi \sim -\pi/2$. In this limit, the inertial correction is negligible (no term involving $a\bar{c}_f$). In figure 5, the dashed and solid lines superpose in this limit.

For larger wavenumber, $Fr\bar{c}_f/2 \ll k\bar{h} \ll \sqrt{\bar{c}_f/2}$, where the second inequality is required for the flow to be fully developed, the bottom shear stress is strongly affected by the inertial correction. In the classical formulation ($a\bar{c}_f = 0$) the shear-stress disturbance is given by

$$\frac{\hat{\tau}}{\bar{\tau}} \sim \frac{2(1+b)}{1-Fr^2}\,\frac{\hat{y}_b}{\bar{h}}. \tag{5.16}$$

The phase angle is $\phi \sim 0^-$ for $Fr < 1$ (figure 5*b*, dashed line) and $\phi \sim -\pi$ for $Fr > 1$ (figure 5*d*, dashed line): the phase angle is negative for all wavenumbers and Froude numbers. In the consistent formulation (non-zero $a\bar{c}_f$), ϕ becomes positive beyond some critical wavenumber k_c for subcritical Froude number (figure 5*b*, solid line), whereas it remains negative for all wavenumbers for supercritical Froude number (figure 5*d*). The large-$k\bar{h}$ limit of the shear-stress disturbance is given by

$$\frac{\hat{\tau}}{\bar{\tau}} \sim \mathrm{i}\,\frac{4a\,k\bar{h}}{(1-Fr^2)/Fr_c^2}\,\frac{\hat{y}_b}{\bar{h}}, \tag{5.17}$$

which shows that the phase angle tends to $\phi = \pi/2$ for $Fr < Fr_c$ and $\phi = -\pi/2$ for $Fr > Fr_c$ (notice, however, that this limit is achieved outside the range of validity of the present theory).

We can conclude that for $Fr < Fr_c$, there exists a critical wavenumber k_c below which the phase angle is negative and above which it is positive. The value of this critical wavenumber can be obtained from (5.14) by imposing a real shear-stress disturbance, and is given by

$$(k_c\bar{h})^2 = \frac{(2+b)(3+b)\bar{c}_f}{8a\left(Fr^{-2} - Fr_c^{-2}\right)}. \tag{5.18}$$

For $Fr > Fr_c$, the phase angle is always negative, with and without the inertial correction. Here is the main conclusion of this section: for subcritical Froude number ($Fr < Fr_c$, where Fr_c is given by (5.10)), ignoring the inertial correction (4.15) of the bottom shear stress implies negative phase angle ϕ; taking into account this correction strongly changes the picture: the phase angle becomes positive for all wavenumbers larger than k_c.

6. Conclusion

The main aim of this paper was to provide quantitative expressions of the phase lead of shear stress in fully developed flow, which is important for its destabilizing effects on the dynamics of an erodible bed. A similar phase lead has long been known to occur for waves short enough that their effect is confined to a thin boundary layer. It was numerically observed to also occur at larger wavelengths, but no general relationship was, to our knowledge, previously derived.

It is important to clarify the parameter range in which the present analysis applies. First, the longitudinal length (and time) scale of the disturbance has to be large compared to typical channel depth. This assumption, $h/L \ll 1$, places the analysis in the general framework of the boundary-layer *equations* (and in so doing excludes the possibility of separated flow). Next our analysis requires the perturbation to reach the surface, i.e. the perturbed as well as unperturbed flow to be fully developed. (The opposite limit of a perturbation confined near the wall had already been studied and is outside the scope of the present paper.) The condition determining such behaviour is $(h/L)Re \ll 1$ in laminar and $(h/L)c_f^{-1/2} \ll 1$ in turbulent flow. The possible regimes are illustrated in table 1. Finally, in part of the analysis we have used the defect-layer concept, which is itself an asymptotic expansion in powers of $c_f^{1/2}$.

The analysis led us to reformulate the widely used Saint-Venant equations (mass and momentum equations for a plug flow with a friction term). Luchini & Charru (2010) had previously shown that a laminar-flow problem satisfying the above assumptions can be consistently formulated if the momentum equation is replaced by a suitable form of the Bernoulli kinetic-energy balance. Whereas for laminar flow the new formulation is exact (as also illustrated in § 3), extending it to turbulent flow requires certain additional assumptions, in particular an algebraic turbulence model (not differently, in this respect, from the unbounded-flow analyses already available in the literature). Interestingly though, the precise form of the turbulent eddy viscosity does not appear in the final result, which is only expressed through integrals of the mean-velocity profile.

At a deeper level, it turns out that the inclusion of friction in the equations of motion is inevitably tied to a departure of the velocity profile from flatness. While this is obvious for laminar flow, it was not *a priori* granted for turbulent flow, which

at least in principle can indefinitely approach a plug flow when $Re \to \infty$ and the wall is smooth. Nonetheless, deviation from flatness appears in the inertial terms with a weight of $(u_\tau/U)^2$, and thus happens to be proportional to c_f just like the friction term. Therefore, even in a formal mathematical limit of $Re \to \infty$ ($c_f \to 0$), it is inconsistent to include one without the other.

This said, both friction and inertial-term corrections have a relatively minor practical effect on those wave phenomena that are governed by the interaction of pressure with gravity. This was brought out in §§ 5.3–5.4. Completely different is the situation when shear stress itself is the objective of study, because then a correction proportional to $c_f h_x$ superposes onto a background that is already of the order of c_f. Indeed, it was shown in § 5.5 that in this case the consistent theory predicts a phase lead that was absent in the classical theory.

The dynamics of shear stress is typically important for the slow evolution of erodible beds, with the formation of ripples and dunes. Indeed, as long as separation does not occur and a linearized analysis applies, provided that the sediment transport rate is in phase with the shear stress (i.e. transport relaxation effects are negligible), bedforms grow when the phase of the shear stress disturbance is positive and decay when the phase angle is negative. Quantitative prediction of the out-of-phase shear stress, or equivalently of the phase lead, is therefore of crucial importance, as it has long been recognized for turbulent flow (Engelund & Fredsøe 1982; Colombini 2004) and for laminar flow as well (Charru 2006). Similar remarks hold for the similar problem of the evolution of a thin viscous film sheared by a gas flow. The results presented here should be relevant for further understanding of these phenomena.

Appendix. The turbulent velocity perturbation profile

The method adopted in § 4 has allowed pressure and shear-stress corrections to be determined without any knowledge of the actual velocity-perturbation profile. Nothing impedes, however, the velocity perturbation from being calculated, should it turn out to be of interest. This appendix is devoted to doing so in the case of a stationary height modulation.

The first step in our previous variable-viscosity analysis was the determination of an equivalent eddy viscosity from a given unperturbed velocity profile $u^{(0)}(y)$. Although the unperturbed velocity distribution (4.12) may at first seem very simplistic, it actually gives rise to a reasonable eddy viscosity. In fact, combining (4.12) with (4.5) gives

$$\nu = -\kappa u_\tau h\, z(1+z). \tag{A 1}$$

This is a parabola that vanishes at both the no-slip and stress-free boundaries, just as a mixing-length argument may suggest. Experiments by Nezu & Rodi (1986) confirm that deviations of the observed turbulent viscosity from a parabola, though measurable, are reasonably small. The non-zero derivative of (4.12) at the free surface is no more worrisome than its infinity at the solid wall already is: both concern only the defect layer and must not be compared with the physical boundary condition but only be used for matching with a suitable wall layer.

A.1. *Wall layer*

There are two ways in which the asymptotic separation into a wall layer and a defect layer can be applied to the present problem of slow height modulations (or, for that matter, to any problem). One is a dimensional argument that only uses this separation in order to specify the non-dimensional groupings appropriate to each

region. This is sufficient to determine the functional dependence of, for instance, the friction coefficient on the Reynolds number up to a couple undetermined constants, which are then to be experimentally measured. The second approach actually writes differential equations for each region and solves them. The first approach is very robust and gives results such as Prandtl's friction law to a very close tolerance but requires data fitting; the second leaves no constants to be determined but carries the uncertainties of closure models.

For the wall layer the traditional argument is a dimensional one and says that, since the scale of this small region is independent of h or its variations, there can exist only one dimensionally consistent velocity profile (the 'universal law of the wall'), where u/u_τ is a function of $(h+y)u_\tau/\nu$ and asymptotes to

$$u/u_\tau \sim B + \kappa^{-1}\log[(h+y)u_\tau/\nu] \tag{A 2}$$

for $(h+y)u_\tau/\nu \to \infty$. In other words, the wall layer is too thin to have any significant dynamics. There is no point then in trying to write a differential equation for its (non-)evolution, and everybody just uses experimentally determined values of the two constants κ and B. More precisely the x-derivative of u_τ, once non-dimensionalized in wall units as $\nu u_{\tau,x}/u_\tau^2$, is Re_τ times smaller than $u_{\tau,x}$ non-dimensionalized with h, and thus exponentially small in the context of an expansion whose parameter is $u_\tau/U \simeq 1/\log(Re_\tau)$ (Mellor 1972). This argument may fail near points of separation where $u_\tau = 0$, but such failure is of no concern here as we only intend to consider mild deviations from parallel flow.

The constants in (A 2) may be taken at their traditional values $\kappa = 0.40$ and $B = 5$ or any more recent revision (Zanoun, Durst & Nagib 2003). Possible wall roughness, which will very often be relevant in practice, can be accounted for by changing the value of B as in the standard theory of channel flow. In the fully rough limit, when roughness height exceeds $\approx 50\nu/u_\tau$, (A 2) becomes independent of viscosity and can be rewritten as

$$u/u_\tau \sim C + \kappa^{-1}\log[(h+y)/h_r], \tag{A 3}$$

where h_r is a representative roughness height and C another constant whose value depends on the precise definition of h_r.

A.2. *Defect layer*

In order to determine the velocity perturbation in the defect layer, the boundary-layer equations (2.1) must be solved with the eddy viscosity (A 1) and boundary conditions stating that

$$v(x,0) = v(x,-h) = 0, \tag{A 4a}$$

$$\lim_{y\to -h}(y+h)u_y = \kappa^{-1}u_\tau, \tag{A 4b}$$

$$\lim_{y\to 0} yu_y = 0. \tag{A 4c}$$

It was already remarked that in turbulent, as in laminar, flow there are two distinct limits giving rise to the same boundary-layer equations: in the classical boundary layer the x-scale is externally imposed and the y-scale is implicitly determined by the parameter u_τ/U (i.e. the y-scale is smaller than the x-scale by a factor of u_τ/U); in channel flow the y-scale is given and the x-scale is implicitly determined to be larger. Contrary to the laminar case, though, two different scale parameters survive in the turbulent channel-flow problem: the fluctuation-intensity parameter u_τ/U

that governs the separation between wall layer and defect layer, and the externally imposed rate of variation of the bottom, which determines the characteristic scale in the x-direction and time. Equations (2.1) with boundary conditions (A 4) must be understood as the result of two independent expansions with respect to both of these parameters.

Boundary conditions (A 4a) are the standard ones for v and, just as in the case of laminar flow, indirectly determine the value of P_x in the momentum equation (2.1b). Condition (A 4b) replaces the no-slip condition of the complete problem with the requirement that the velocity profile should tend to its characteristic logarithmic behaviour in a neighbourhood of $y=-h$. More precisely, it imposes the asymptotic behaviour of the velocity derivative, while leaving a free additive constant in u to be determined later by matching with the wall layer. On the free surface, condition (A 4c) imposes zero shear stress (but not necessarily zero velocity gradient, because viscosity tends to zero as far as the defect layer is concerned).

For the zeroth-order problem, a straight duct, (2.1b) reduces to $\rho^{-1}P_x=(\nu u_y)_y$ and unsurprisingly for the viscosity distribution (A 1) its solution is exactly (4.12) together with $v^{(0)}=0$ and $P_x^{(0)}=-\rho u_\tau^2/h$.

The perturbation problem is introduced next by assuming that channel height is a function $h(x)$ with a typical scale of variation asymptotically large compared to h itself, so that h_x is small, and that consequently (4.12) remains valid as a zeroth-order solution but with U and u_τ now functions of x.

First-order continuity formally determines the requirement that $\int_{-h}^{0}u^{(0)}\,\mathrm{d}y=Q=hU=\text{const.}$, and thus determines $U(x)$ as a function of $h(x)$. The other parameter $u_\tau(x)$ must also be regarded as externally assigned as far as the defect layer is concerned; its final value will only be known once an additional constraint is imposed on it by matching with the wall layer.

Also at first order, the momentum equation (2.1b) and boundary conditions (A 4) become

$$\left(\nu u_y^{(1)}\right)_y-\rho^{-1}P_x^{(1)}=u^{(0)}u_x^{(0)}+v^{(1)}u_y^{(0)}=u^{(0)}u_x^{(0)}-u_y^{(0)}\int_0^y u_x^{(0)}\,\mathrm{d}y, \tag{A 5}$$

$$v^{(1)}(0)=v^{(1)}(-h)=0;\quad \lim_{y\to0}yu_y^{(1)}=\lim_{y\to-h}(y+h)u_y^{(1)}=0, \tag{A 6}$$

with $P_x^{(1)}$ implicitly determined so that $\int_{-h}^{0}u^{(1)}\,\mathrm{d}y=0$ (a compatibility condition for second-order continuity). Since u_τ/U is assumed to be asymptotically small and (2.1b) represents, in turbulent flow, the first term of an expansion in powers of u_τ/U, we are authorized to neglect $O(u_\tau^2)$ contributions on the right-hand side of (A 5), thus writing

$$\left(\nu u_y^{(1)}\right)_y-\rho^{-1}P_x^{(1)}=UU_x+U\delta u_x^{(0)}+U_x\left(\delta u^{(0)}-y\delta u_y^{(0)}\right), \tag{A 7}$$

where $\delta u^{(0)}=\kappa^{-1}u_\tau[1+\log(1+y/h)]$. (The $O(u_\tau^2)$ correction to pressure will be lost, however. Had we not performed it already by other means, the calculation of pressure would require quadratic terms to be retained.) Thence, after changing variable from y to $z=y/h(x)$,

$$h^{-2}\left(\nu u_z^{(1)}\right)_z-\rho^{-1}P_x^{(1)}=UU_x+\kappa^{-1}(Uu_\tau)_x[1+\log(1+z)]-\frac{(Uh_x/h+U_x)u_\tau z}{\kappa(1+z)}. \tag{A 8}$$

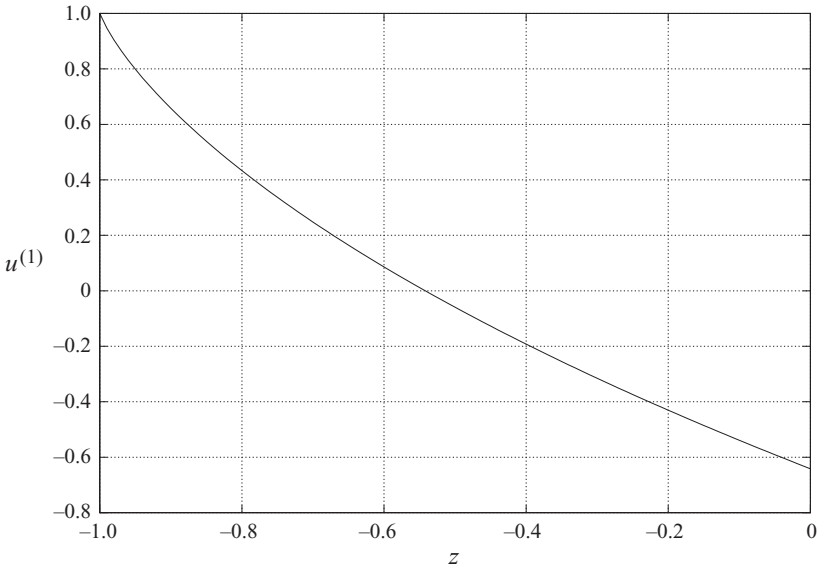

FIGURE 6. First-order velocity correction (A 10).

Since hU is a constant, the factor $Uh_x/h + U_x = 0$ and the corresponding term can thus be deleted. Integrating once and then replacing ν by its expression (A 1) yields

$$z(1+z)u_z^{(1)} = \frac{h(Uu_\tau)_x}{\kappa^2 u_\tau}\,[C_2 + C_1 z + (1+z)\log(1+z)], \tag{A 9}$$

where $\kappa^{-1}(Uu_\tau)_x C_1 = UU_x + \rho^{-1}P_x^{(1)}$. The two last boundary conditions of (A 6) require $C_1 = C_2 = 0$. After a second integration

$$u^{(1)} = \frac{h(Uu_\tau)_x}{\kappa^2 u_\tau}\left(C_3 + \int_0^z \frac{\log(1+z)}{z}\,\mathrm{d}z\right). \tag{A 10}$$

The remaining constant C_3 must now be derived from the requirement of zero flow rate for $u^{(1)}$ (which, from a formal viewpoint, stems from the continuity equation at order 2). Its value, obtainable through a detour into complex-path integration, is $1 - \pi^2/6$. The resulting profile of the first-order velocity $u^{(1)}(z)$ is shown in figure 6.

In order to complete the matching with the wall layer and confirm the calculation of the wall-shear stress given in § 4.3, the single value $u^{(1)}(-1)$ is all we shall actually need. Imposing

$$\int_0^{-1} u^{(1)}\,\mathrm{d}z = u^{(1)}(-1) - \int_0^{-1} z u_z^{(1)}\,\mathrm{d}z = 0, \tag{A 11}$$

where $u_z^{(1)}$ is to be taken from (A 9), gives

$$u^{(1)}(-1) = \frac{h(Uu_\tau)_x}{\kappa^2 u_\tau}. \tag{A 12}$$

A.3. *Matching*

The matching condition between wall layer and defect layer requires that the asymptotic behaviour for $(h+y)/h \to 0$ of the latter be equated to the asymptotic behaviour (A 2) for $(h+y)u_\tau/\nu \to \infty$ of the former. Writing $u = u^{(0)} + u^{(1)}$, where

$u^{(1)}$ has a finite limit for $z \to -1$, and using the expression (4.12) of $u^{(0)}$ produces the condition that

$$U + \kappa^{-1} u_\tau \left[1 + \log\left(\frac{h+y}{h}\right)\right] + u^{(1)}(-1) = B u_\tau + \kappa^{-1} u_\tau \log\left(u_\tau \frac{h+y}{\nu}\right) \tag{A 13}$$

i.e. using (A 12),

$$\frac{U}{u_\tau} + \frac{h(Uu_\tau)_x}{\kappa^2 u_\tau^2} = B + \kappa^{-1}\left[\log\left(\frac{h u_\tau}{\nu}\right) - 1\right] \tag{A 14}$$

or the corresponding expression for the roughness-dominated regime if (A 3) is used in the place of (A 2).

By observing that for $(Uu_\tau)_x = 0$ the result must be the zeroth-order value of U/u_τ (related to the friction coefficient in a straight duct), one can combine both cases of a negligible or non-negligible roughness in a single formula by writing

$$\frac{U}{u_\tau} + \frac{h(Uu_\tau)_x}{2\kappa^2 u_\tau^2} = \left(\frac{U}{u_\tau}\right)^{(0)} = \left(\frac{2}{c_f}\right)^{1/2}, \tag{A 15}$$

where for the smooth-wall regime

$$(2/c_f)^{1/2} = B + \kappa^{-1}[\log(h u_\tau/\nu) - 1] \tag{A 16}$$

and for the fully rough regime

$$(2/c_f)^{1/2} = C + \kappa^{-1}[\log(h/h_r) - 1]. \tag{A 17}$$

In the coefficient $(Uu_\tau)_x/u_\tau^2$, u_τ can (to first order in the perturbative expansion) be replaced by $u_\tau^{(0)} = (c_f/2)^{1/2} U$. Neglecting at the same time the x-derivative of c_f, which according to either (A 16) or (A 17) turns out to be of a higher order in u_τ/U, gives

$$(Uu_\tau)_x/u_\tau^2 \simeq (c_f/2)^{1/2}(U^2)_x/u_\tau^2 \simeq (c_f/2)^{-1/2} 2U_x/U. \tag{A 18}$$

Therefore, (A 15) becomes

$$U/u_\tau \simeq (c_f/2)^{-1/2}(1 - \kappa^{-2} h U_x/U) \tag{A 19}$$

or, upon taking its reciprocal square,

$$\tau_w \simeq (1 + 2\kappa^{-2} h U_x/U)\tau_w^{(0)} = (1 - 2\kappa^{-2} h_x) c_f \rho U^2/2, \tag{A 20}$$

which coincides with the formerly derived result (4.15) of § 4.3.

REFERENCES

Abrams, J. & Hanratty, T. J. 1985 Relaxation effects observed for turbulent flow over a wavy surface. *J. Fluid Mech.* **151**, 443–455.

Aradian, A., Raphael, É. & de Gennes, P. G. 2002 Surface flows of granular materials: a short introduction to some recent models. *C.R. Phys.* **3**, 187–196.

Balmforth, N. J. & Mandre, S. 2004 Dynamics of roll waves. *J. Fluid Mech.* **514**, 1–33.

Batchelor, G. K. 1967 *An Introduction to Fluid Dynamics*. Cambridge University Press.

Belcher, S. E. & Hunt, J. C. R. 1998 Turbulent flow over hills and waves. *Annu. Rev. Fluid Mech.* **30**, 507–538.

Benjamin, T. B. 1959 Shearing flow over a wavy boundary. *J. Fluid Mech.* **6**, 161–205.

Brock, R. R. 1969 Development of roll-wave trains in open channels. *J. Hydr. Div. ASCE* **95-HY4**, 1401–1427.

Chang, H.-C. & Demekhin, E. A. 2002 *Complex Wave Dynamics on Thin Films*. Elsevier.

Charru, F. 2006 Selection of the ripple length on a granular bed sheared by a liquid flow. *Phys. Fluids* **18**, 121508.

Colombini, M. 2004 Revisiting the linear theory of sand dune formation. *J. Fluid Mech.* **502**, 1–16.

Engelund, F. 1970 Instability of erodible beds. *J. Fluid Mech.* **42**, 225–244.

Engelund, F. & Fredsøe, J. 1982 Sediment ripples and dunes. *Annu. Rev. Fluid Mech.* **14**, 13–37.

Forterre, Y. & Pouliquen, O. 2008 Flows of dense granular media. *Annu. Rev. Fluid Mech.* **40**, 1–24.

Gradowczyk, M. H. 1968 Wave propagation and boundary instability in erodible-bed channels. *J. Fluid Mech.* **33**, 93–112.

Hinze, J. O. 1975 *Turbulence*. McGraw Hill.

Hopfinger, E. J. 1983 Snow avalanche motion and related phenomena. *Annu. Rev. Fluid Mech.* **15**, 47–76.

Jackson, P. S. & Hunt, J. C. R. 1975 Turbulent wind flow over a low hill. *Q. J. R. Meteorol. Soc.* **101**, 929–955.

Jeffreys, H. 1925 The flow of water in an inclined channel of rectangular cross-section. *Phil. Mag.* (6) **49**, 793–807.

Jimenez, J., Uhlmann, M., Pinelli, A. & Kawahara, G. 2001 Turbulent shear flow over active and passive porous surfaces. *J. Fluid Mech.* **442**, 89–117.

Julien, P. Y. & Hartley, D. M. 1986 Formation of roll waves in laminar sheet flow. *J. Hydraul. Res.* **24**, 5–17.

Lin, P. Y. & Hanratty, T. J. 1986 Prediction of the initiation of slugs with linear stability theory. *Intl J. Multiphase Flow* **12**, 79–98.

Luchini, P. & Charru, F. 2010 Consistent section-averaged equations of quasi-one-dimensional laminar flow. *J. Fluid Mech.* **656**, 337–341.

Mellor, G. L. 1972 The large Reynolds number, asymptotic theory of turbulent boundary layers. *Intl J. Engng Sci.* **10**, 851–873.

Needham, D. J. & Merkin, J. H. 1984 On roll waves down an open inclined channel. *Proc. R. Soc. Lond.* A **394**, 259–278.

Nezu, I. & Rodi, W. 1986 Open-channel flow measurements with a laser Doppler anemometer. *J. Hydr. Engng* **112**, 335–355.

Pedlosky, J. 2003 *Waves in the Ocean and Atmosphere*. Springer.

Richards, K. J. 1980 The formation of ripples and dunes on an erodible bed. *J. Fluid Mech.* **99**, 597–618.

de Saint-Venant, A. J. C. B. 1871 Théorie du mouvement non-permanent des eaux, avec application aux crues des rivières et à l'introduction des marées dans leur lit. *C. R. Acad. Sci. Paris* **73**, 147–154, 237–240.

Sumer, B. M. & Bakioglu, M. 1984 On the formation of ripples on an erodible bed. *J. Fluid Mech.* **144**, 177–190.

Usha, R. & Uma, B. 1994 Modeling of stationary waves on a thin viscous film down an inclined plane at high Reynolds numbers and moderate Weber numbers using energy integral method. *Phys. Fluids* **16**, 2679–2696.

Whitham, G. B. 1974 *Linear and Nonlinear Waves*. Wiley.

Zanoun, E.-S., Durst, F. & Nagib, H. 2003 Evaluating the law of the wall in two-dimensional fully developed turbulent channel flows. *Phys. Fluids* **15**, 3079–3089.